

The effect of peculiar velocities on the epoch of reionization (EoR) 21-cm signal

Suman Majumdar^{1,2*}, Somnath Bharadwaj^{1†} and T. Roy Choudhury^{3‡}

¹Department of Physics and Meteorology & Centre for Theoretical Studies, IIT, Kharagpur 721302, India

²Department of Astronomy & Oskar Klein Centre, AlbaNova, Stockholm University, SE-106 91 Stockholm, Sweden

³National Centre for Radio Astrophysics, TIFR, Post Bag 3, Ganeshkhind, Pune 411007, India

24 June 2013

ABSTRACT

We have used semi-numerical simulations of reionization to study the behaviour of the power spectrum of the EoR 21-cm signal in redshift space. We have considered two models of reionization, one which has homogeneous recombination (HR) and the other incorporating inhomogeneous recombination (IR). We have estimated the observable quantities — quadrupole and monopole moments of H I power spectrum at redshift space from our simulated data. We find that the magnitude and nature of the ratio between the quadrupole and monopole moments of the power spectrum (P_2^s/P_0^s) can be a possible probe for the epoch of reionization. We observe that this ratio becomes negative at large scales for $\bar{x}_{\text{H I}} \leq 0.7$ irrespective of the reionization model, which is a direct signature of an inside-out reionization at large scales. It is possible to qualitatively interpret the results of the simulations in terms of the fluctuations in the matter distribution and the fluctuations in the neutral fraction which have power spectra and cross-correlation $P_{\Delta\Delta}(k)$, $P_{xx}(k)$ and $P_{\Delta x}(k)$ respectively. We find that at large scales the fluctuations in matter density and neutral fraction is exactly anti-correlated through all stages of reionization. This provides a simple picture where we are able to qualitatively interpret the behaviour of the redshift space power spectra at large scales with varying $\bar{x}_{\text{H I}}$ entirely in terms of a just two quantities, namely $\bar{x}_{\text{H I}}$ and the ratio $P_{xx}/P_{\Delta\Delta}$. The nature of $P_{\Delta x}$ becomes different for HR and IR scenarios at intermediate and small scales. We further find that it is possible to distinguish between an inside-out and an outside-in reionization scenario from the nature of the ratio P_2^s/P_0^s at intermediate length scales.

Key words: methods: data analysis - cosmology: theory: - diffuse radiation

1 INTRODUCTION

The epoch when the neutral hydrogen (H I) in the inter-galactic medium (IGM) was reionized by the first luminous sources, is one of the least known periods in the history of our universe. Observations of the CMBR (Spergel et al., 2003; Page et al., 2007; Komatsu et al., 2011; Larson et al., 2011) and absorption spectra of high redshift quasars (Becker et al., 2001; Fan et al., 2003; White et al., 2003; Fan et al., 2006; Willott et al., 2007; Goto et al., 2011) suggest that the epoch of reionization (EoR) probably extended over the redshift range $6 \leq z \leq 15$ (Fan et al., 2006; Choudhury & Ferrara, 2006; Alvarez et al., 2006; Mitra et al., 2011). However these observations are limited in their ability to shed light on many important questions regarding EoR. What are the major sources of reionization? What are the typical sizes and the topology of the ionized regions at different stages? Observations of redshifted 21-cm

radiation from neutral hydrogen hold the promise to answer some of these questions. The brightness temperature of the redshifted 21-cm radiation directly probes the H I distribution at the epoch where the radiation originated. It is thus possible to track the entire reionization history as it gradually proceeds with redshift. The presently functioning low frequency radio telescopes GMRT¹ (Swarup et al., 1991), LOFAR² and 21CMA³, the upcoming MWA⁴ and the future SKA⁵ all cover the frequency range relevant for the EoR 21-cm signal, and this is one of the major goals for most of these telescopes. It is therefore very important to have a good picture of the expected signal in order to make forecasts for and correctly interpret the future observations of the redshifted 21-cm radiation.

There has been a considerable amount of work towards simulating the expected EoR 21-cm signal. In particular, there have been

* E-mail: sumanm@phy.iitkgp.ernet.in

† E-mail: somnath@phy.iitkgp.ernet.in

‡ E-mail: tirth@ncra.tifr.res.in

¹ <http://www.gmrt.ncra.tifr.res.in>

² <http://www.lofar.org/>

³ <http://21cma.bao.ac.cn/>

⁴ <http://www.haystack.mit.edu/ast/arrays/mwa/>

⁵ <http://www.skatelescope.org/>

numerical simulations which use ray-tracing to follow the propagation of ionization fronts in the IGM (Gnedin, 2000; Ciardi et al., 2001; Ricotti et al., 2002; Razoumov et al., 2002; Maselli et al., 2003; Sokasian et al., 2003; Iliev et al., 2006; Mellema et al., 2006; McQuinn et al., 2007; Trac & Cen, 2007; Semelin et al., 2007; Shin et al., 2008; Iliev et al., 2008; Shapiro et al., 2008; Thomas et al., 2009; Baek et al., 2009). Such simulations are computationally extremely expensive, and it is difficult to simulate large volumes, and to re-run the simulations considering different values of the simulation parameters. Semi-numerical simulations which consider the average photon density in place of a detailed ray-tracing analysis provide a computationally less expensive technique to simulate the EoR 21-cm signal (Furlanetto et al., 2004; Mesinger & Furlanetto, 2007; Geil & Wyithe, 2008; Lidz et al., 2009; Choudhury et al., 2009; Alvarez et al., 2009; Santos et al., 2010; Mesinger et al., 2011; Zahn et al., 2011).

The fluctuations in the brightness temperature of the redshifted 21-cm radiation essentially trace the H I distribution during EoR. The redshift space distortion caused by peculiar velocities also plays an important role in shaping the redshifted 21-cm signal (Bharadwaj et al., 2001; Bharadwaj & Ali, 2004). In fact, we expect the peculiar velocities to introduce an anisotropy in the three dimensional power spectrum of the EoR 21-cm signal (Barkana & Loeb, 2005; Bharadwaj & Ali, 2005; Wang & Hu, 2006), very similar to the characteristic anisotropy present in the galaxy power spectrum (Kaiser, 1987). Barkana & Loeb (2005) have proposed that it may be possible to use this anisotropy to separate the effect of the peculiar velocities from the other astrophysical information present in the 21-cm power spectrum.

Until recently, most simulations of the EoR 21-cm signal have not considered the effect of redshift space distortions. Some of the earlier work Mellema et al. (2006) and Thomas et al. (2009) have considered this effect while generating H I maps through their simulations, but have not studied its implication on the statistical properties like the power spectrum of the brightness temperature fluctuations. Recently, Santos et al. (2010) and Mesinger et al. (2011) have included the effect of redshift space distortions in an approximate, perturbative fashion in their semi-numerical simulation and used this to study its implications on the redshifted 21-cm brightness temperature power spectrum at different stages of the reionization. In a very recent work Mao et al. (2012) discuss the methodology to implement redshift space distortion in numerical simulations of reionization, and used this to study the 21-cm brightness temperature power spectrum during EoR.

Most of the earlier semi-numerical simulations (*e.g.* Furlanetto et al. 2004; Mesinger & Furlanetto 2007; Geil & Wyithe 2008; Lidz et al. 2009; Alvarez et al. 2009; Santos et al. 2010; Mesinger et al. 2011; Zahn et al. 2011) have assumed spatially homogeneous recombination which predicts strictly inside-out reionization where the most dense regions ionize first, the ionization subsequently propagating to lower densities. However, there are observations which indicate exactly opposite picture at the end of reionization, where the high density regions remain neutral (due to self-shielding) and the low density regions are highly ionized. Choudhury et al. (2009) have attempted to make their semi-numerical simulation consistent with these observations by incorporating the fact that recombination occurs faster in high density regions. In these simulations reionization is inside-out only in the early stages. However, self-shielded, high density clumps remain neutral in the later stages of reionization when inhomogeneous recombination is taken into account. In this paper we follow Choudhury et al. (2009) to develop a semi-numerical code to simulate reionization, with the fur-

ther improvement that we incorporate the effect of redshift space distortion due to peculiar velocities. We have used these simulations to study the effect of peculiar velocities on the EoR 21-cm signal, both with homogeneous recombination and with inhomogeneous recombination.

In this paper we have used semi-numerical simulations to determine the EoR 21-cm signal at different stages of reionization, and used the H I power spectrum to quantify the statistical properties of this signal. We have calculated $P_{H\text{ I}}^r(k)$ the H I power spectrum in real space and its redshift space counterpart $P_{H\text{ I}}^s(\mathbf{k})$, and compared these two to assess the effect of peculiar velocities. The anisotropy of the 21-cm signal, quantified through various angular multipoles of $P_{H\text{ I}}^s(\mathbf{k})$, is a very useful tool to study the effect of redshift space distortion. In particular, we have studied the monopole and quadrupole moments of $P_{H\text{ I}}^s(\mathbf{k})$ in order to identify the features characteristic of redshift space distortion at different stages of reionization. To our knowledge, this anisotropy has not been quantified using simulations in any of the earlier studies. Finally, we attempt to interpret the results of our simulations, and compare these against the predictions of the simple, linear model proposed by Barkana & Loeb (2005).

Unless mentioned otherwise, throughout this paper we present results for the cosmological parameters $h = 0.704$, $\Omega_m = 0.272$, $\Omega_\Lambda = 0.728$, $\Omega_b h^2 = 0.0226$ (all parameters from WMAP 7 year data (Komatsu et al., 2011; Jarosik et al., 2011)).

A brief summary of the paper follows. In Section 2, we present the semi-numerical technique that we have used to simulate the EoR 21-cm signal including the effect of peculiar velocities. Section 3, contains a brief discussion of the model prediction for the effect of redshift space distortion. These were used as reference values in presenting and interpreting the results from our simulations in Section 4. Finally, we discuss our results and conclude in Section 5.

2 SIMULATING REDSHIFT SPACE DISTORTION DURING REIONIZATION

We have used a semi-numerical simulation to generate the H I ionization map during reionization. The simulation essentially starts from the dark matter distribution at a given redshift, and uses this to identify the sources of ionizing photons. These sources, along with the assumption that the H I traces the dark matter are used to construct a snapshot of the H I ionization distribution. Our simulation is based on the formalism proposed by Choudhury et al. (2009). This uses an excursion-set formalism as introduced by Furlanetto et al. (2004). The semi-numerical simulation provides us with the ionization field in the real space *i.e.* without the redshift space distortion. We briefly discuss the semi-numerical method that we have used in this work to simulate the brightness temperature fluctuations of the redshifted 21-cm emission from EoR.

We have used a Particle Mesh N-body code to generate the dark matter distribution. The spatial and mass resolution of the N-body simulation should be adequate to correctly resolve all the ionizing sources that one is going to adopt in this semi-numerical simulation. It is currently believed that the stars residing in the galaxies are the major source of photons to reionize the universe (Yan & Windhorst, 2004; Stiavelli et al., 2004; Bouwens et al., 2005; Fan et al., 2006; Choudhury & Ferrara, 2006). The presently accepted models suggest that dark matter halos having a mass $M \geq 10^9 h^{-1} M_\odot$ host the early galaxies that contribute to reionization. We thus include all dark matter halos of mass $M \geq 10^9 h^{-1} M_\odot$ in

our semi-numerical simulation. Assuming that at least 10 dark matter particles are required to constitute the smallest halo, the N-body simulation is required to have a mass resolution $\leq 10^8 h^{-1} M_\odot$.

We have generated the dark matter distribution at $z = 8$ using the Particle Mesh N-body code. The volume of the simulation is constrained by the 16 Gigabytes of memory available in our computer. We perform our simulation in a periodic box of size 85.12 Mpc (comoving) with 1216^3 grid points and 608^3 particles, with a mass resolution $M_{part} = 7.275 \times 10^7 h^{-1} M_\odot$.

We identify halos within the simulation box using a standard Friend-of-Friend algorithm (Davis et al., 1985), with a fixed linking length 0.2 (in units of mean inter particle distance) and minimum dark matter halo mass $= 10M_{part}$.

The relation between the ionizing luminosity of a galaxy and its properties is not well known from the observations. In the semi-numerical formalism adopted here, we assume that the ionizing luminosity from a galaxy is proportional to the mass of its halo. The number of ionizing photons contributed by a halo of mass M is given by

$$N_\gamma(M) = N_{ion} \frac{M}{m_H} \quad (1)$$

where m_H is the mass of a hydrogen atom and N_{ion} is a dimensionless constant. The value of N_{ion} is tuned so as to achieve the desired mass-averaged neutral fraction in the simulation. The ionizing photon field is estimated on a grid which has a resolution 8 times coarser than the N-body simulation.

In our simulation we assume that the baryons follow the dark matter distribution and we also assume that each N-body particle has same hydrogen mass M_H . In the semi-numerical formalism, a region is said to be ionized if the average number of photons reaching there exceeds the average neutral hydrogen density at that point. Before applying the ionization condition we assume that the entire hydrogen contained in each particle is completely neutral. Using this assumption we calculate the H I density field in the same grid where the photon field has been generated. The photon and the H I density at each grid point are compared and a neutral fraction $x_{H\ I}$ is assigned to the grid point depending on the ionization conditions discussed below.

In this work we consider two different models of reionization. In one model the recombination rate is assumed to be homogeneous (HR) and independent of density throughout the IGM. In the other model we have considered a density dependent inhomogeneous recombination (IR). Readers are requested to refer to the Section 2 of Choudhury et al. (2009) for further details of ionization conditions (eq. [7] and [15] of Choudhury et al. 2009) in these two different models of reionization. For the simulation results related to IR model presented in this paper we have set the inhomogeneous recombination parameter $\epsilon = 1.0$ (see Section 2.5 and eq. [15] of Choudhury et al. 2009 for the definition of ϵ).

We next discuss how we implement the effect of peculiar velocities on the ionization maps generated. We first consider the dark matter particles to each of which we have assigned a total hydrogen mass M_H . The ionization map provides us with a neutral fraction $x_{H\ I}$ at each grid point of the simulation. For the i th particle in the simulation, we have interpolated the neutral fraction from its eight nearest neighbouring grid points to determine the neutral fraction $x_{H\ I}^i$ at the particle's position. We use this to calculate the particle H I mass $M_{H\ I}^i$ as

$$M_{H\ I}^i = x_{H\ I}^i M_H. \quad (2)$$

This provides us with the H I distribution and the peculiar velocity

associated with each H I element. We now consider a distant observer located along the x axis, and use the x component of the peculiar velocity to determine the particle positions in redshift space

$$s = x + \frac{v_x}{aH(a)} \quad (3)$$

where a and $H(a)$ are the scale factor and Hubble parameter respectively. Finally we have interpolated the H I distribution from the particles to the grid, and used this to generate the EoR 21-cm signal. This method of mapping the real space H I density in redshift space is some what similar to the PPM-RRM scheme discussed in Mao et al. (2012).

3 MODELING REDSHIFT SPACE DISTORTION DURING REIONIZATION

Coherent inflows into overdense regions and outflows from underdense regions appear as enhancements in the matter density fluctuations observed in redshift space. This introduces an anisotropy (Kaiser, 1987) in $P^s(k, \mu)$ the redshift space matter power spectrum

$$P^s(k, \mu) = (1 + \mu^2)^2 P^r(k) \quad (4)$$

where $P^r(k)$ is the real space power spectrum and $\mu = \mathbf{k} \cdot \hat{\mathbf{n}}/k$ is the cosine of the angle between the wave vector \mathbf{k} and the unit vector $\hat{\mathbf{n}}$ along the line of sight (LoS). Here we have assumed $\Omega_m = 1$ throughout, which is reasonable at the high redshifts of our interest. It is convenient (Hamilton, 1992, 1998; Cole et al., 1995) to decompose the anisotropy using Legendre polynomials $\mathcal{P}_l(\mu)$ as

$$P^s(k, \mu) = \sum_{l \text{ even}} \mathcal{P}_l(\mu) P_l^s(k), \quad (5)$$

where $P_l^s(k)$ are the different angular multipoles of $P^s(k, \mu)$. Under the linear approximation (eq. 4), only the first three even moments have non-zero values $P_0^s(k)/P^r(k) = 28/15$, $P_2^s(k)/P^r(k) = 40/21$ and $P_4^s(k)/P^r(k) = 8/35$ which are constant independent of k .

Peculiar velocities have a similar effect on the brightness temperature fluctuations ΔT_b of the 21-cm H I radiation from the high redshift universe (Bharadwaj et al., 2001; Bharadwaj & Ali, 2004). Expressing the brightness temperature fluctuations as $\Delta T_b(\mathbf{x}, z) = \bar{T}(z) \eta_{H\ I}(\mathbf{x}, z)$ and considering the EoR where the spin temperature is much higher than the CMBR temperature ($T_S \gg T_\gamma$) we have (Bharadwaj & Ali, 2005)

$$\eta_{H\ I}(\mathbf{x}, z) = \frac{\rho_{H\ I}}{\bar{\rho}_H} \left[1 - \frac{(1+z)}{H(z)} \frac{\partial v_{\parallel}}{\partial r} \right] \quad (6)$$

where all the quantities in the r.h.s. refer to the position and epoch where the H I emission originated and $\bar{T}(z) = 4.0 \text{ mK} (1+z)^2 \left(\frac{\Omega_b h^2}{0.02} \right) \left(\frac{0.7}{h} \right) \frac{H_0}{H(z)}$. Here $\rho_{H\ I}$ refers to the H I density (which varies from position to position), $\bar{\rho}_H$ is the mean hydrogen density, r is the comoving distance from the observer and v_{\parallel} is the radial component of the peculiar velocity. We may express $\rho_{H\ I}$ using $\rho_{H\ I}/\bar{\rho}_H = x_{H\ I} (1 + \delta)$ where $x_{H\ I}$ is the hydrogen neutral fraction and δ is the matter overdensity which we have assumed to be the same as the hydrogen overdensity at the large length-scales of our interest. Further, we may express the neutral fraction as $x_{H\ I} = \langle x_{H\ I} \rangle_V (1 + \delta_x)$ where $\langle x_{H\ I} \rangle_V$ is the volume averaged neutral fraction and δ_x is the contrast in the $x_{H\ I}$ distribution. Note that the volume averaged neutral fraction $\langle x_{H\ I} \rangle_V$ and the mass averaged neutral fraction $\bar{x}_{H\ I}$ refer to the average of $x_{H\ I}$ and

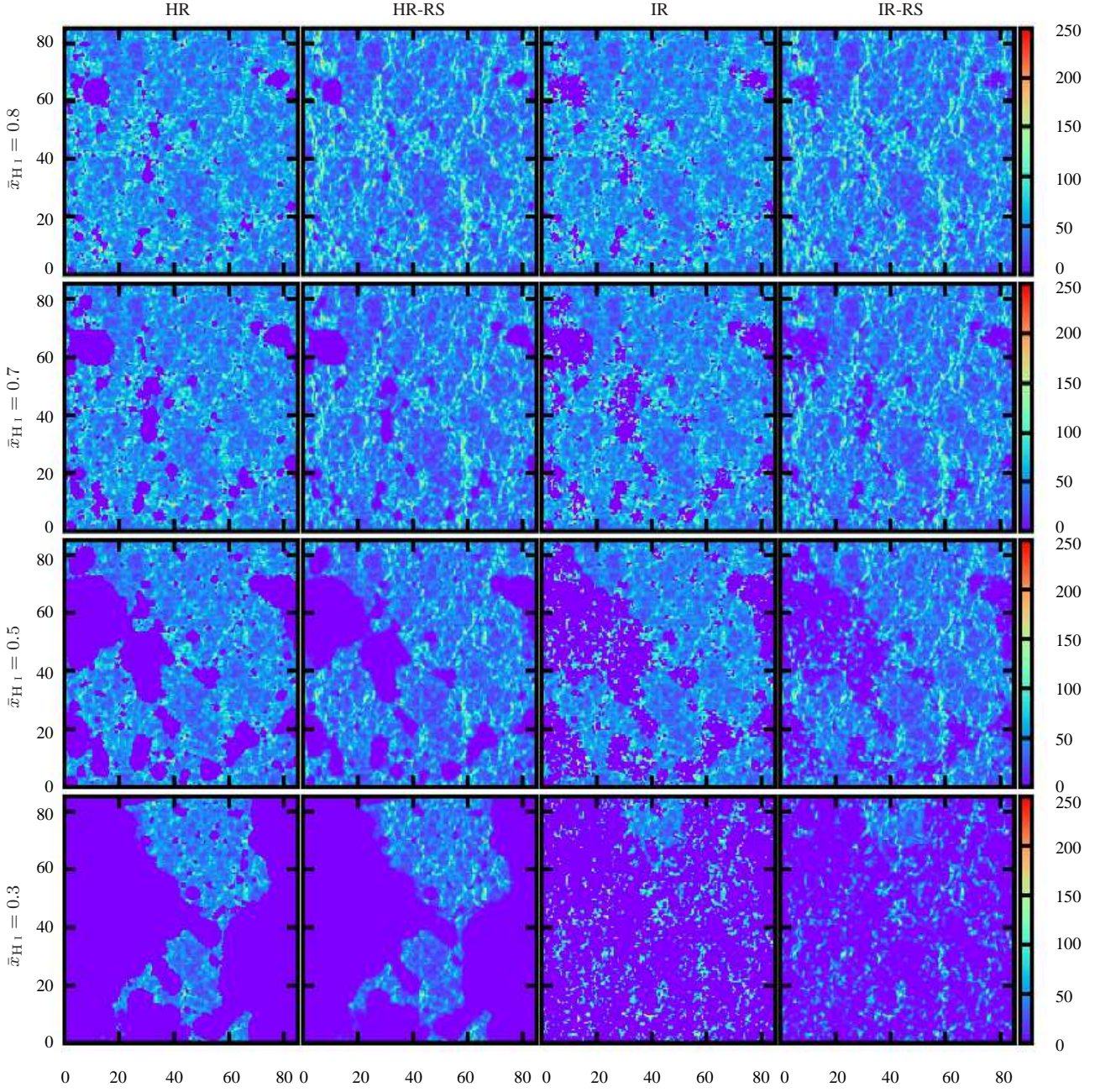


Figure 1. Simulated H I maps in real and redshift space with different schemes of reionizations for various values of $\bar{x}_{H\text{I}}$. In this figure we use HR, HR-RS, IR and IR-RS to denote homogeneous recombination, homogeneous recombination with redshift space distortion, inhomogeneous recombination and inhomogeneous recombination with redshift space distortion respectively. The line of sight is along the x-axis and the coordinates are in Mpc. The colour index represents H I density in arbitrary units.

$x_{H\text{I}}(1 + \delta)$ respectively. Assuming that $\delta_x, \delta, (\partial v_{\parallel} / \partial r) \ll 1$ we drop all quadratic and higher terms involving δ_x, δ and $(\partial v_{\parallel} / \partial r)$, to obtain $\langle x_{H\text{I}} \rangle_V = \bar{x}_{H\text{I}}$ whereby it is possible to express $\eta_{H\text{I}}$ in Fourier space as

$$\tilde{\eta}_{H\text{I}}(\mathbf{k}) = \bar{x}_{H\text{I}} [\Delta_x + (1 + \mu^2)\Delta]. \quad (7)$$

where $\tilde{\eta}_{H\text{I}}, \Delta$ and Δ_x are the Fourier transform of $\eta_{H\text{I}}, \delta$ and δ_x respectively. This gives the redshift space H I power spectrum (of

$\eta_{H\text{I}}$) to be (Barkana & Loeb, 2005)

$$P_{H\text{I}}^s(k, \mu) = \bar{x}_{H\text{I}}^2 [P_{xx}(k) + 2(1 + \mu^2)P_{\Delta x}(k) + (1 + \mu^2)^2 P_{\Delta\Delta}(k)] \quad (8)$$

where P_{xx} and $P_{\Delta\Delta}$ are the power spectra of Δ_x and Δ respectively, and $P_{\Delta x}$ is the cross power spectrum between Δ and Δ_x . We recover the real space H I power spectrum $P^r(k)$ if we set $\mu = 0$ in eq. (8). Here, and in the subsequent discussion, we drop the subscript H I for brevity of the symbols. Thus the H I power spectrum

in real space will be

$$P^r = \bar{x}_{H\text{I}}^2 (P_{\Delta\Delta} + 2P_{\Delta x} + P_{xx}). \quad (9)$$

In this model only the first three even angular moments of the redshift space power spectrum have non-zero values

$$P_0^s = \bar{x}_{H\text{I}}^2 \left(\frac{28}{15} P_{\Delta\Delta} + \frac{8}{3} P_{\Delta x} + P_{xx} \right), \quad (10)$$

$$P_2^s = \bar{x}_{H\text{I}}^2 \left(\frac{40}{21} P_{\Delta\Delta} + \frac{4}{3} P_{\Delta x} \right), \quad (11)$$

$$P_4^s = \bar{x}_{H\text{I}}^2 \left(\frac{8}{35} \right) P_{\Delta\Delta}. \quad (12)$$

To provide an interpretation of our results obtained from semi-numerical simulations in this paper we have used this linear model. Finally, we note that this model is based on the assumption $\delta_x \ll 1$, and terms of the order of $\delta_x \delta$ which appear in eq. (6) are ignored. While this is possibly a reasonable assumption in the early stages of reionization ($\bar{x}_{H\text{I}} \sim 1$), we may expect significant deviations from this model in the late stages of the reionization where $\bar{x}_{H\text{I}}$ is small and we expect δ_x to exhibit large fluctuation of order unity. Lidz et al. (2007) and Mao et al. (2012) have considered models which incorporate the non-linear effects, but these are rather complicated and we have not attempted using these models here.

3.1 Method to estimate the angular multipoles of H I power spectrum from the simulated H I maps

We Fourier transform the entire simulated image data cube and estimate the angular multipoles P_l^s of H I power spectrum from the Fourier transformed data following the equation

$$P_l^s(k) = \frac{(2l+1)}{4\pi} \int \mathcal{P}_l(\mu) P^s(k) d\Omega, \quad (13)$$

where $P^s(k)$ is the H I power spectrum in the redshift space which has been estimated from the Fourier transform of the simulated redshift space H I map. The integral is done over the entire solid angle to take into account all possible orientations of the \mathbf{k} vector with the LoS direction $\hat{\mathbf{n}}$. Each angular multipole is estimated at 10 logarithmically spaced k bins in the range $0.09 \leq k \leq 4.80 \text{ Mpc}^{-1}$.

4 RESULTS

We have simulated the H I distribution, in both real and redshift space, for $\bar{x}_{H\text{I}}$ values starting from 1.0 to 0.1 with an interval of $\Delta\bar{x}_{H\text{I}} = 0.1$. For each value of $\bar{x}_{H\text{I}}$ we have used 12 independent realizations⁶ of the simulation to estimate the mean and 1σ error of the H I power spectrum. The simulations are all carried out at a fixed redshift $z = 8$. Ideally, one should adopt a model for the evolution of $\bar{x}_{H\text{I}}$ with z and simulate each neutral fraction at the appropriate redshift. This, however, makes the results dependent on the model for the redshift evolution of $\bar{x}_{H\text{I}}$ and also makes the computations rather cumbersome. We have sidestepped this issue by keeping z fixed at a value $z = 8$ which is in the redshift range that is considered favourable for observing the EoR 21-cm signal.

However due to this approach we are unable account for the evolution for the dark matter density field as well the evolution of the sources of ionizing photons in our simulation. We interpret the simulations for different values of $\bar{x}_{H\text{I}}$ as representing different stages of reionization.

Figure 1 shows the H I distributions at different stages of reionization in both real and redshift space for a single realization of the simulation. We see that the H I distributions in the HR and the IR models are nearly indistinguishable in the early stages of reionization ($\bar{x}_{H\text{I}} \geq 0.7$). In the early stages reionization proceeds inside-out in both of these models with the high density regions ionizing first and the low density regions ionizing later. The H I maps of the two models become quite distinct at the later stages of reionization ($\bar{x}_{H\text{I}} \leq 0.5$). In the IR model we find many small isolated neutral H I clumps distributed within the regions which are completely ionized in the HR model. These small H I clumps correspond to the high density regions which become self-shielded due to the enhancement in the recombination rate in the IR model. Comparing the real and redshift space H I maps we see that in the initial stages the ionized and neutral regions respectively appear slightly contracted and elongated along the LoS. For the HR model the H I distribution exhibits the same behaviour even in the late stages. The small H I clumps which appear in the late stages of the IR model however, show the opposite behaviour. These neutral regions appear contracted along the LoS. All the features mentioned above can be understood based on the fact that overdense and underdense regions respectively appear contracted and elongated along the LoS.

We show the ratio between the monopole of the redshift space power spectrum with its real space counterpart in Figure 2. This ratio (P_0^s/P^r) has been extensively used in the literature (e.g. Lidz et al. 2007; Mesinger et al. 2011; Mao et al. 2012) to quantify the effect of redshift space distortion. The earlier works have reported that at large length scales this ratio rises to a value greater than 1.87 in the early stages of reionization, and then falls to a value slightly less than 1 at later stages. Our results show a similar behaviour in both the HR and IR models. We also find that at large length scales ($k \sim 0.2 \text{ Mpc}^{-1}$) P_0^s/P^r rises to a value ≈ 2 at $\bar{x}_{H\text{I}} = 0.8 - 0.9$ and then abruptly falls to a value slightly less than 1 at $\bar{x}_{H\text{I}} = 0.7$. The ratio subsequently rises gradually and approaches 1 as $\bar{x}_{H\text{I}}$ decreases. The behaviour at intermediate length scales ($k \sim 0.5 \text{ Mpc}^{-1}$) is somewhat similar, except that we have a sharp peak at $\bar{x}_{H\text{I}} = 0.9$. Also, the ratio again exceeds 1 at $\bar{x}_{H\text{I}} \leq 0.2$ for the IR model. Several earlier works have highlighted the initial rise in P_0^s/P^r at $\bar{x}_{H\text{I}} \sim 0.8$ as a very prominent feature of the effect of redshift space distortion on the EoR 21-cm signal. We note, that the expected signal itself drops considerably at $\bar{x}_{H\text{I}} = 0.8$ and this is possibly not very significant from the observational point of view. Further, the sudden rise in P_0^s/P^r is possibly because of the rapid decline in the signal itself (due to the possible negative contribution from $P_{\Delta x}$ in eq. [9] and competition between $P_{\Delta\Delta}$, $P_{\Delta x}$ and P_{xx} , this is further verified later in this paper in Figure 5 and 6) at $\bar{x}_{H\text{I}} = 0.8$. Both P_0^s and P^r reduces at this stage, however P^r , which appears in the denominator of this ratio, declines much faster than P_0^s (for further details see the relevant discussion in Mao et al. 2012).

The quantity that in principle can be directly estimated from the observational data and will quantify the strength as well as the nature of the redshift space anisotropy is the ratio between the quadrupole and the monopole of the redshift space power spectrum. Our estimations for this ratio (P_2^s/P_0^s) from simulations has been shown in the Figure 3. We find that for $\bar{x}_{H\text{I}} = 1.0$ the results

⁶ All the results shown here (Figure 2 to 6) are mean estimated from these 12 independent realizations.

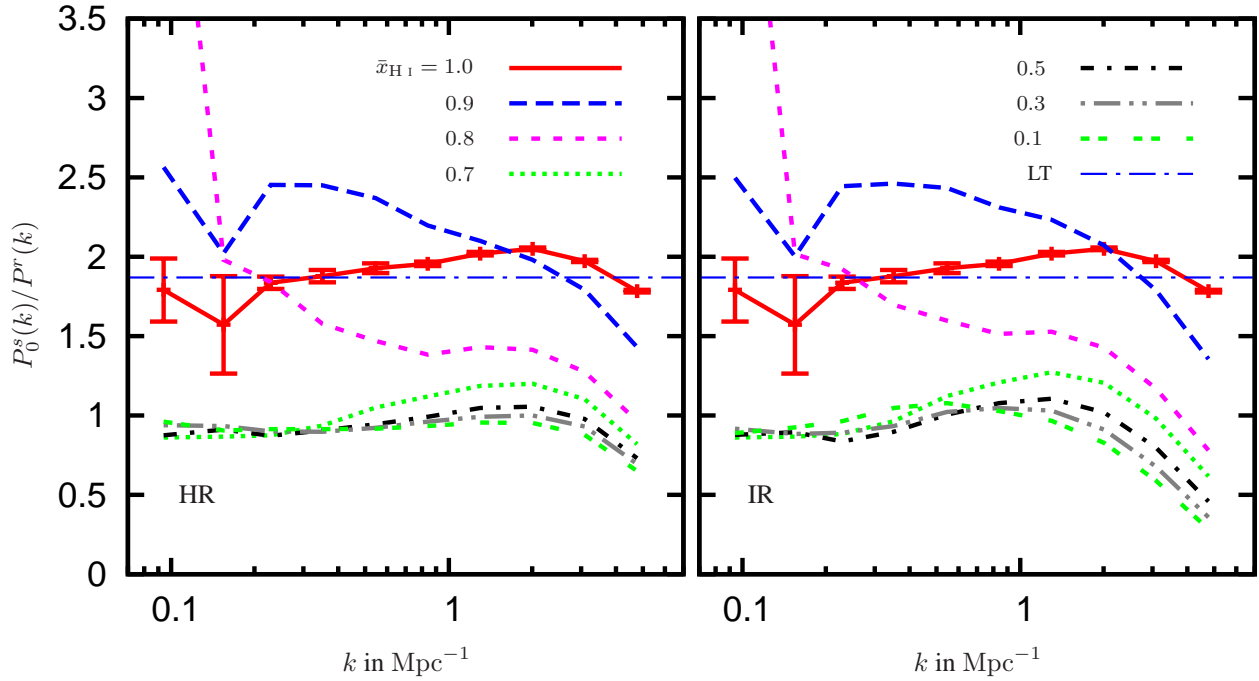


Figure 2. The ratio $P_0^s(k)/P^r(k)$ for different neutral fractions and for both the models of reionization. For reference, the horizontal thin dash-dot line (LT) shows the value $28/15$ predicted by the linear theory of redshift space distortion for a completely neutral IGM. The error bars represent the 1σ sample variance estimated from 12 independent realizations.

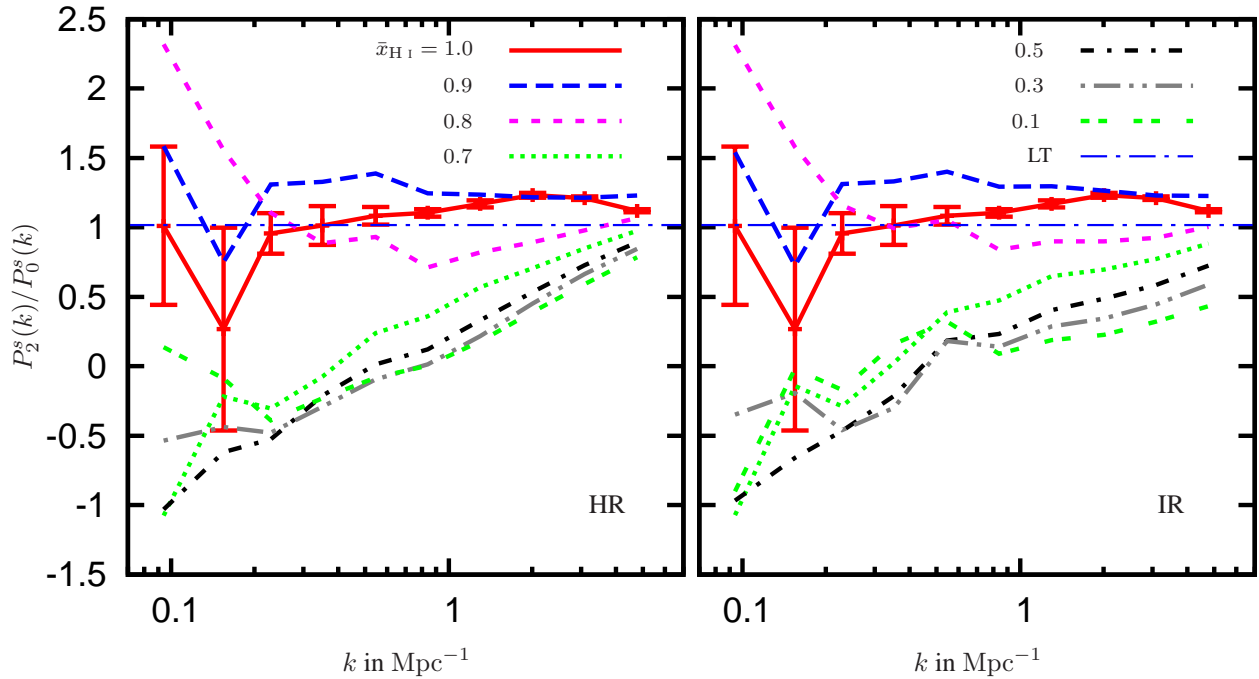


Figure 3. The ratio $P_2^s(k)/P_0^s(k)$ for different neutral fractions and for both the models of reionization. For reference, the horizontal thin dash-dot line (LT) shows the value $50/49$ predicted by the linear theory of redshift space distortion for a completely neutral IGM. The error bars represent the 1σ sample variance estimated from 12 independent realizations.

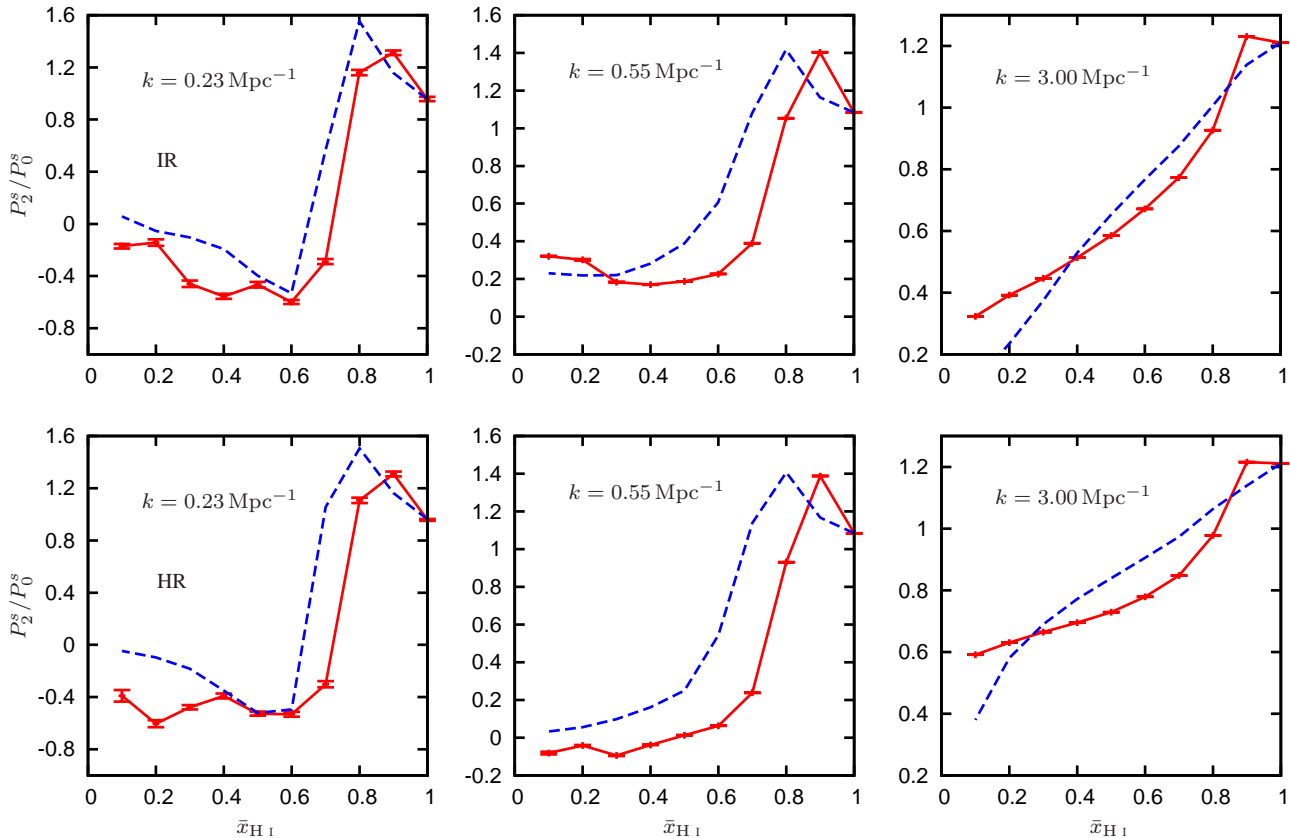


Figure 4. The ratio P_2^s/P_0^s as a function of \bar{x}_{H1} for the three mentioned values of the wave number k . The simulation (thick solid line) are compared with the model prediction (dashed line). The error bars are estimated following the analysis discussed in Appendix A, excluding the effects from any specific telescope.

from our simulations are consistent with the value 1.02 predicted by linear theory at large length scales ($k \leq 0.5 \text{ Mpc}^{-1}$). At smaller scales the ratio is larger than 1.02 possibly because of the non-linear redshift space distortion. This ratio increases at all length scales for $\bar{x}_{H1} = 0.9$. The ratio increases further for $\bar{x}_{H1} = 0.8$ at large scales ($k < 0.3 \text{ Mpc}^{-1}$) whereas it decreases at smaller length scales. The behaviour of this ratio changes significantly at $\bar{x}_{H1} \leq 0.7$ where we find that P_2^s/P_0^s is negative at large scales. The value increases steadily as we move to smaller scales, crosses zero at $k \sim 1.0 \text{ Mpc}^{-1}$ and is positive at smaller length scales. The results for the HR and IR models are very similar except that there is a bump at around $k \sim 0.5 \text{ Mpc}^{-1}$ for the IR model. To understand the evolution of P_2^s/P_0^s with \bar{x}_{H1} in more detail we study the behaviour of this ratio as a function of \bar{x}_{H1} (Figure 4) at three representative k modes $k = 0.23, 0.55$ and 3.00 Mpc^{-1} hitherto referred to as large, intermediate and small scales. We could have, in principle, chosen a smaller k mode to illustrate the behaviour at large scales. The errors however are rather large for $k < 0.2 \text{ Mpc}^{-1}$ and these scales do not provide a very reliable estimate of the behaviour, and we need larger simulations to study the behaviour at length scales as large as these. Considering the large scale first (Figure 4), the behaviour of the HR and IR models are both quite similar. The ratio rises from ~ 1 at $\bar{x}_{H1} = 1.0$ to 1.4 at $\bar{x}_{H1} = 0.8 - 0.9$ and then abruptly falls to ≈ -0.3 at $\bar{x}_{H1} = 0.7$. The ratio remains negative with values in the range $(-0.4) - (-0.6)$ for smaller values of \bar{x}_{H1} with the exception that it rises to ≈ -0.2 for $\bar{x}_{H1} \leq 0.2$ in the IR model. The behaviour at intermediate scales is very similar as that at the large

scales except that the ratio falls to a value in the range $0.2 - 0.4$ at $\bar{x}_{H1} = 0.7$ instead of becoming negative. The ratio declines further and is negative (≈ -0.1) for $\bar{x}_{H1} < 0.4$ in the HR model. In the IR model the ratio is negative nowhere and is in the range $0.2 - 0.4$ for $\bar{x}_{H1} < 0.7$. At small scales the ratio is constant at ~ 1.2 for $\bar{x}_{H1} \geq 0.9$ where after it falls rapidly to 0.8 at $\bar{x}_{H1} = 0.7$ and subsequently declines gradually to ~ 0.6 and ~ 0.4 in the HR and IR models respectively.

The hexadecapole $P_4^s(k)$ measured from our simulations has very large error bars, and consequently we have not shown these here. Larger simulations are required for reliable estimates of $P_4^s(k)$. However it can be noted that the linear model predicts the ratio $P_4^s(k)/P_0^s(k)$ to be very small ($P_4^s/P_0^s \simeq 0.12$) even for a completely neutral IGM, when compared with the ratio $P_2^s/P_0^s \simeq 1.02$. Thus a successful estimation of $P_4^s(k)$ from the observational data is intrinsically a difficult task. A recent work by Shapiro et al. (2013) has discussed the validity of using the 4th moment of the redshift space power spectrum (in μ decomposition technique), which is somewhat similar to the hexadecapole $P_4^s(k)$, for extracting the cosmological information from the redshifted 21 cm observations.

5 DISCUSSION AND CONCLUSIONS

We first compare our results with the predictions of the model discussed in Section 3 for which P_0^s and P_2^s can be calculated using eq.s (10) and (11) respectively. The model requires $P_{\Delta\Delta}(k)$,

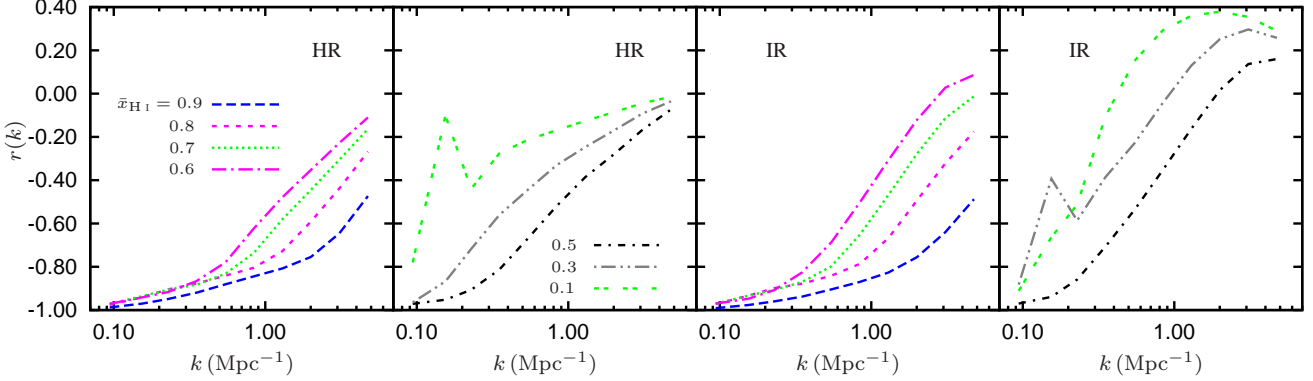


Figure 5. The dimensionless cross-correlation $r(k)$ for different neutral fractions and for both the models of reionization.

$P_{xx}(k)$ and $P_{\Delta x}(k)$ which we have directly determined from our simulations at different stages of reionization. Several earlier authors (Lidz et al., 2007; Mesinger et al., 2011; Mao et al., 2012) have noted that this model does not correctly reproduce the real and redshift space power spectrum P^r and P_0^s determined from simulations. Our results for the $\bar{x}_{\text{H I}}$ dependence of P_2^s/P_0^s shown in Figure 4 confirm that the model fails to quantitatively reproduce the results of the simulations. We however note that the predictions of this model are qualitatively very similar to the results of the simulations, and this provides a very useful framework for interpreting our results. In the subsequent discussion we have used the framework of this model to discuss and qualitatively interpret the $\bar{x}_{\text{H I}}$ dependence of the observable quantity P_2^s/P_0^s , which we have studied earlier.

According to the linear model the quantities which will combinedly determine the strength as well as the nature of the redshift space distortions are the cross-correlation power spectrum ($P_{\Delta x}$) between the matter density fluctuations (Δ) and the fluctuations in the neutral fraction (Δ_x) and the power spectrum of fluctuations in the neutral fraction field (P_{xx}). The quantity P_{xx} by definition will always be positive, whereas the quantity $P_{\Delta x}$ can have both positive or negative values. A negative/positive contribution from $P_{\Delta x}$ would represent an anti-correlation/correlation between the Δ and Δ_x fields. To understand their relative contribution on the simulated redshift space power spectrum we represent them in terms of two dimensionless quantities

$$\mathcal{A}(k) = \sqrt{P_{xx}(k)/P_{\Delta\Delta}(k)}, \quad (14)$$

and

$$r(k) = P_{\Delta x}(k)/\sqrt{P_{xx}(k)P_{\Delta\Delta}(k)}, \quad (15)$$

from our simulations. The quantity $\mathcal{A}(k)$ defines the relative amplitude of P_{xx} with respect to $P_{\Delta\Delta}$, whereas $r(k)$ determines the strength of cross-correlation between Δ and Δ_x . Figure 5 and 6 show $r(k)$ and $\mathcal{A}(k)$ respectively at different stages of reionization. Considering the large scales first we find that $r \simeq -1$ at all stages of reionization in both the HR and IR models. This indicates that at large scales the distribution of neutral fraction is anti-correlated with the matter distribution throughout reionization, this being a consequence of the fact that the high density regions are the locations where we expect to find the sources that drives reionization thus they are expected to get ionized first and only the low density regions remain neutral. Note that the small neutral clumps produced at the later stages in the IR model do not affect this behaviour seen at large scales. At all scales we find $\mathcal{A}(k)$ to mono-

tonically increase with decreasing $\bar{x}_{\text{H I}}$. The observed sharp peak of the ratio P_2^s/P_0^s (left panels of Figure 4) at the early stages of reionization ($\bar{x}_{\text{H I}} \simeq 0.9$) at large and intermediate scales thus represent the fact that at this stage the contribution from P_{xx} becomes comparable to $P_{\Delta\Delta}$ and due to a complete anti-correlation between Δ and Δ_x (*i.e.* $r \simeq -1$) the actual signal (P_0^s) becomes very low, which appears at the denominator of this ratio. This peak thus should not be misinterpreted as a signature of redshift space distortion. At the later stages of reionization ($0.1 < \bar{x}_{\text{H I}} \leq 0.8$ for the HR and $0.3 < \bar{x}_{\text{H I}} \leq 0.8$ for the IR model) the cross correlation still remains $r \simeq -1$ whereas $P_{xx} > P_{\Delta\Delta}$ which leads to a negative value of P_2^s/P_0^s in both models of reionization. These results points towards an inside-out reionization at large scales. We observe that the presence of small neutral clumps, produced at the later stages in the IR model, does not contribute significantly at the large scale power spectrum. Thus a negative value of P_2^s/P_0^s of the 21-cm power spectrum itself will be a direct evidence that the reionization has happened and it is inside-out at large scale.

The fluctuations in the neutral fraction $\Delta_x(k)$ and the matter $\Delta(k)$ are not perfectly anti-correlated ($r > -1$) at intermediate and small scales. The value of r increases as we go to smaller scales, and the behaviour is similar in the HR and IR models at the early stages of reionization ($\bar{x}_{\text{H I}} \geq 0.8$). We see differences between the HR and IR model at intermediate and small scales at the later stages of reionization. The values of r are larger in the IR model in comparison to the HR model, and r becomes positive at small scales in the later stages in the IR model whereas it is nowhere positive in the HR model. This difference is the outcome of the small H I clumps seen in Figure 1 at the later stages in the IR model. The signature of this difference is also visible in the observed power spectrum (P_2^s/P_0^s) at the intermediate scales (middle panels of Figure 4). At intermediate scales the ratio P_2^s/P_0^s becomes negative during the later stages of reionization ($\bar{x}_{\text{H I}} \leq 0.6$) in the HR model, however in IR model it never becomes negative at these scales and more or less maintains a constant positive value of ≈ 0.2 at the later stages of reionization.

Thus the two major signatures from the redshift space 21-cm signal that can be used as the evidence of reionization as well as a characterization for the redshift space anisotropy are the following

- A negative value of the ratio P_2^s/P_0^s at large scales during the intermediate and late stages of reionization.
- The ratio P_2^s/P_0^s stays negative even at intermediate scales for

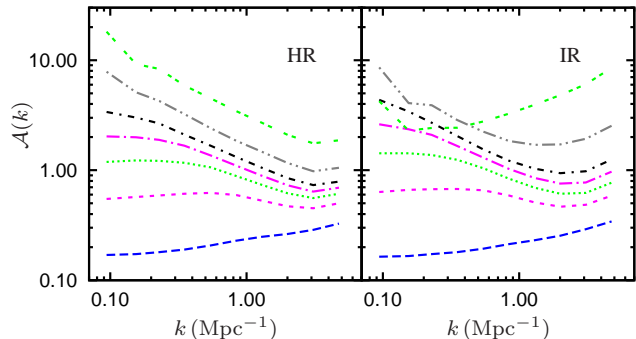


Figure 6. This shows $\mathcal{A}(k) = \sqrt{P_{xx}(k)/P_{\Delta\Delta}(k)}$ for different neutral fractions and for both the models of reionization. The line styles are the same as Figure 5. In the left panel the bottom most curve corresponds to $\bar{x}_{\text{HI}} = 0.9$ and the value of $\mathcal{A}(k)$ increases monotonically with decreasing \bar{x}_{HI} .

a completely inside-out reionization whereas it becomes positive for a partially outside-in reionization.

The main point of concern here is how unambiguously it will be possible to detect these signatures, or in other words what level of sensitivity our measurements will require to detect these signatures. To get an idea of the accuracy level of the measurements required and to find out the possible effects of uncertainty, we have done a rough error analysis for estimations of the ratios of various angular multipoles. This analysis has been discussed in detail in Appendix A. Following this analysis (eq. [A18]) we have estimated the possible errors in our estimation of the ratio P_2/P_0 and shown them as error bars in Figure 4. However while estimating these errors we have not considered the possible uncertainties arising from the system noise of a specific observation with a telescope and also replaced the cosmic variance in eq. (A18) with the sample variance of the zeroth moment of the power spectrum. We plan to include the effect of system noise and various other observation specific effects in our future work. From our analysis in Appendix A and results in Figure 4 it is evident that it will be possible to unambiguously detect both these signatures of reionization at large and intermediate scales, to which the present (*e.g.* LOFAR, see Jensen et al. (2013) for more details) and upcoming telescopes will be sensitive, if the system noise can be suppressed to a sufficient level.

Another alternative approach to quantify the strength and the nature of redshift space distortion from the H I power spectrum is by decomposing the redshift space power spectrum in the various coefficients of the powers of μ . These estimated coefficients can be then interpreted following a linear (Barkana & Loeb, 2005) or a quasi-linear (Mao et al., 2012) model. However in this method the estimated coefficients of the powers of μ will not be completely independent of each other and the correlation between them (or the leakage of power from one component to another) may give rise to wrong interpretations as observed in a recent work by Jensen et al. (2013). In comparison to this method the decomposition of the anisotropy due to peculiar velocities using Legendre polynomials, is a representation in orthonormal basis therefore the various angular multipoles estimated through this method will be independent of each other (as discussed in Appendix A). Thus one does not have to be too concerned about the leakage of power between different multipoles in this method.

It is anticipated that the initial observational attempts (*e.g.* GMRT, LOFAR and MWA) will probe the EoR 21-cm signal only

at large scales. The multipole moments of the power spectrum of the measured signal hold the key to quantify and interpret it. We have considered the ratio between the quadrupole and monopole moments which is capable of quantifying the strength of the signal and the anisotropy which arises due to the peculiar velocities. Our simulations indicate that the prospects of detecting the EoR 21-cm signal are most favourable when the mean neutral fraction is in the range $\bar{x}_{\text{HI}} = 0.4-0.5$. In this range the signal, we see, is characterized by two main features for both the HR and IR models of reionization. First, the monopole moment of the redshift space H I power spectrum $P_0^s(k)$ is nearly equal to the real space H I power spectrum $P^r(k)$, and both of these are comparable to the real space matter power spectrum. Second, the quadrupole moment of the redshift space H I power spectrum $P_2^s(k)$ is negative with a value which is -0.5 times $P_0^s(k)$. This is in contrast to the value 1.02 predicted by linear theory for the ratio P_2^s/P_0^s of the matter power spectrum. We also observe that it would be possible to distinguish between the inside-out and the outside-in reionization scenarios from the nature of the ratio between the quadrupole and monopole moments at the intermediate length scales ($k \simeq 0.5 \text{ Mpc}^{-1}$). This particular signature may help in ruling out the extremely outside-in reionization models using future observations.

6 ACKNOWLEDGMENTS

Suman Majumdar would like to thank Prof. Sugata Pratik Khastgir for useful discussions and pointing out some errors in the initial version of the manuscript. Suman Majumdar would like to acknowledge Council of Scientific and Industrial Research (CSIR), India for providing financial assistance through a senior research fellowship (File No. 9/81 (1099)/10-EMR-I).

References

- Alvarez, M. A., Shapiro, P. R., Ahn, K., & Iliev, I. T. 2006, ApJL, 644, L101
- Alvarez, M. A., Busha, M., Abel, T., & Wechsler, R. H. 2009, ApJL, 703, L167
- Baek, S., Di Matteo, P., Semelin, B., Combes, F., & Revaz, Y. 2009, AAP, 495, 389
- Barkana, R., & Loeb, A. 2005, ApJL, 624, L65
- Becker, R. H., Fan, X., White, R. L., et al. 2001, AJ, 122, 2850
- Bharadwaj, S., Nath, B. B., & Sethi, S. K. 2001, Journal of Astrophysics and Astronomy, 22, 21
- Bharadwaj, S., & Ali, S. S. 2004, MNRAS, 352, 142
- Bharadwaj, S., & Ali, S. S. 2005, MNRAS, 356, 1519
- Bouwens, R. J., Illingworth, G. D., Thompson, R. I., & Franx, M. 2005, ApJL, 624, L5
- Cole, S., Fisher, K. B., & Weinberg, D. H. 1995, MNRAS, 275, 515
- Choudhury, T. R., Ferrara, A., 2006, Cosmic Polarization, Editor - R. Fabbri(Research Signpost), p. 205, arXiv:astro-ph/0603149
- Choudhury, T. R., & Ferrara, A. 2006, Albert Einstein Century International Conference, 861, 835
- Choudhury, T. R., 2009, Current Science, 97, 6, 841
- Choudhury, T. R., Haehnelt, M. G., & Regan, J. 2009, MNRAS, 394, 960
- Ciardi, B., Ferrara, A., Marri, S., & Raimondo, G. 2001, MNRAS, 324, 381

Davis, M., Efstathiou, G., Frenk, C. S., & White, S. D. M. 1985, *ApJ*, 292, 371

Fan, X., Strauss, M. A., Schneider, D. P., et al. 2003, *AJ*, 125, 1649

Fan, X., Carilli, C. L., & Keating, B. 2006, *Annu. Rev. Astro. Astrophys.*, 44, 415

Furlanetto, S. R., Zaldarriaga, M. & Hernquist, L. 2004, *ApJ*, 613, 1

Geil, P. M., & Wyithe, J. S. B. 2008, *MNRAS*, 386, 1683

Gnedin, N. Y. 2000, *ApJ*, 535, 530

Goto, T., Utsumi, Y., Hattori, T., Miyazaki, S., & Yamauchi, C. 2011, *MNRAS*, 415, L1

Hamilton, A. J. S. 1992, *ApJL*, 385, L5

Hamilton, A. J. S. 1998, *The Evolving Universe*, 231, 185

Iliev, I. T., Pen, U.-L., Richard Bond, J., Mellema, G., & Shapiro, P. R. 2006, *New Astronomy Reviews*, 50, 909

Iliev, I. T., Mellema, G., Pen, U.-L., Bond, J. R., & Shapiro, P. R. 2008, *MNRAS*, 384, 863

Jarosik, N., Bennett, C. L., Dunkley, J., et al. 2011, *ApJS*, 192, 14

Jensen, H., Datta, K. K., Mellema, G., et al. 2013, *arXiv:1303.5627*

Kaiser, N. 1987, *MNRAS*, 227, 1

Komatsu, E., Smith, K. M., Dunkley, J., et al. 2011, *ApJS*, 192, 18

Larson, D., Dunkley, J., Hinshaw, G., et al. 2011, *ApJS*, 192, 16

Lidz, A., Zahn, O., McQuinn, M., et al. 2007, *ApJ*, 659, 865

Lidz, A., Zahn, O., Furlanetto, S. R., et al. 2009, *ApJ*, 690, 252

Mao, Y., Shapiro, P. R., Mellema, G., et al. 2012, *MNRAS*, 422, 926

Maselli, A., Ferrara, A., & Ciardi, B. 2003, *MNRAS*, 345, 379

McQuinn, M., Lidz, A., Zahn, O., et al. 2007, *MNRAS*, 377, 1043

Mellema, G., Iliev, I. T., Pen, U.-L., & Shapiro, P. R. 2006, *MNRAS*, 372, 679

Mesinger, A., & Furlanetto, S. 2007, *ApJ*, 669, 663

Mesinger, A., Furlanetto, S., & Cen, R. 2011, *MNRAS*, 411, 955

Mitra, S., Choudhury, T. R., & Ferrara, A. 2011, *MNRAS*, 413, 1569

Page, L., Hinshaw, G., Komatsu, E., et al. 2007, *ApJS*, 170, 335

Razoumov, A. O., Norman, M. L., Abel, T., & Scott, D. 2002, *ApJ*, 572, 695

Ricotti, M., Gnedin, N. Y., & Shull, J. M. 2002, *ApJ*, 575, 33

Santos, M. G., Ferramacho, L., Silva, M. B., Amblard, A., & Cooray, A. 2010, *MNRAS*, 406, 2421

Semelin, B., Combes, F., & Baek, S. 2007, *AAP*, 474, 365

Shapiro, P. R., Iliev, I. T., Mellema, G., Pen, U.-L., & Merz, H. 2008, *The Evolution of Galaxies Through the Neutral Hydrogen Window*, 1035, 68

Shapiro, P. R., Mao, Y., Iliev, I. T., et al. 2013, *Physical Review Letters*, 110, 151301

Shin, M.-S., Trac, H., & Cen, R. 2008, *ApJ*, 681, 756

Sokasian, A., Abel, T., Hernquist, L., & Springel, V. 2003, *MNRAS*, 344, 607

Spergel, D. N., Verde, L., Peiris, H. V., et al. 2003, *ApJS*, 148, 175

Stiavelli, M., Fall, S. M., & Panagia, N. 2004, *ApJL*, 610, L1

Swarup G., Ananthakrishnan S., Kapahi V.K., Rao A.P., Subramanya C.R., Kulkarni V.K., 1991 *Curr.Sci.*, 60, 95

Thomas, R. M., Zaroubi, S., Ciardi, B., et al. 2009, *MNRAS*, 393, 32

Trac, H., & Cen, R. 2007, *ApJ*, 671, 1

Wang, X., & Hu, W. 2006, *ApJ*, 643, 585

White, R. L., Becker, R. H., Fan, X., & Strauss, M. A. 2003, *AJ*, 126, 1

Willott, C. J., Delorme, P., Omont, A., et al. 2007, *AJ*, 134, 2435

Yan, H., & Windhorst, R. A. 2004, *ApJL*, 600, L1

Zahn, O., Lidz, A., McQuinn, M., et al. 2007, *ApJ*, 654, 12

Zahn, O., Mesinger, A., McQuinn, M., et al. 2011, *MNRAS*, 414, 727

APPENDIX A: QUANTIFYING THE POSSIBLE UNCERTAINTIES IN THE ESTIMATION OF ANGULAR MOMENTS OF THE 21-CM POWER SPECTRUM

In this section we provide a rough analysis for quantifying the possible uncertainties in the estimation of angular multipoles of power spectrum and their ratios. We consider redshifted 21-cm observations that cover a 3-D volume V . In the continuum limit, the number of independent Fourier modes dN corresponding to d^3k is

$$dN = V \frac{d^3k}{(2\pi)^3} \quad (\text{A1})$$

We consider $\hat{P}(\mathbf{k})$ which is an unbiased estimator of the power spectrum at the Fourier mode \mathbf{k} . This has the properties that

$$\langle \hat{P}(\mathbf{k}) \rangle = P(\mathbf{k}) \quad (\text{A2})$$

and

$$\langle [\Delta \hat{P}(\mathbf{k})][\Delta \hat{P}(\mathbf{k}')] \rangle = \frac{(2\pi)^3}{V} \delta(\mathbf{k} - \mathbf{k}') \sigma^2(\mathbf{k}) \quad (\text{A3})$$

where the latter equation essentially tells us that the estimates at the different Fourier modes are independent. Also the variance of power spectrum estimator has two independent contributions

$$\sigma^2(\mathbf{k}) = [P(\mathbf{k}) + \sigma_N^2]^2 \quad (\text{A4})$$

which arise from the cosmic variance $[P(\mathbf{k})]$ and the system noise $[\sigma_N^2]$ respectively. The system noise is inherent to the observations and it depends on the observing time, the telescope, etc.

We use this to define estimators for the multipole moments of the power spectrum

$$\hat{P}_n(k_i) = \frac{\int d^3k \mathcal{P}_n(\mu) \hat{P}(\mathbf{k})}{\int d^3k \mathcal{P}_n^2(\mu)} \quad (\text{A5})$$

where $\mathcal{P}_n(\mu)$ is the Legendre polynomial of order n , $\mu = \mathbf{k} \cdot \mathbf{n}/k$ is the cosine of the angle between \mathbf{k} and the line of sight \mathbf{n} , and the d^3k integral is over a spherical shell of radius k_i and width Δk_i .

We have

$$\langle \hat{P}_n(k_i) \rangle = P_n(k_i). \quad (\text{A6})$$

We assume that the bins have no overlap, whereby it is obvious that the estimators $P_n(k_i)$ and $P_m(k_j)$ in two different bins ($k_i \neq k_j$) are uncorrelated. We now calculate the covariance between the multipoles in the same bin

$$\langle [\Delta \hat{P}_n(k_i)][\Delta \hat{P}_m(k_i)] \rangle = \left\langle \frac{\int d^3k_1 \mathcal{P}_n(\mu_1) [\Delta \hat{P}(\mathbf{k}_1)]}{\int d^3k_1 \mathcal{P}_n^2(\mu_1)} \frac{\int d^3k_2 \mathcal{P}_m(\mu_2) [\Delta \hat{P}(\mathbf{k}_2)]}{\int d^3k_2 \mathcal{P}_m^2(\mu_2)} \right\rangle \quad (\text{A7})$$

which using eq. (A3) gives

$$\langle [\Delta \hat{P}_n(k_i)][\Delta \hat{P}_m(k_i)] \rangle = \frac{(2\pi)^3 V^{-1} \int d^3k_1 \mathcal{P}_n(\mu_1) \mathcal{P}_m(\mu_1) \sigma^2(\mathbf{k})}{\int d^3k_1 \mathcal{P}_n^2(\mu_1) \int d^3k_2 \mathcal{P}_m^2(\mu_2)} \quad (\text{A8})$$

This can be further simplified using

$$\int d^3k \mathcal{P}_n(\mu_1) \mathcal{P}_m(\mu_1) \sigma^2(\mathbf{k}) = 2\pi k_i^2 \Delta k_i \sigma^2(k_i) \int_{-1}^1 d\mu_1 \mathcal{P}_n(\mu_1) \mathcal{P}_m(\mu_1) \quad (\text{A9})$$

and

$$\int_{-1}^1 d\mu_1 \mathcal{P}_n(\mu_1) \mathcal{P}_m(\mu_1) = \frac{2\delta_{n,m}}{2n+1} \quad (\text{A10})$$

whereby

$$\langle [\Delta \hat{P}_n(k_i)] [\Delta \hat{P}_m(k_i)] \rangle = \delta_{m,n} \frac{2\pi^2 (2n+1) \sigma^2(k_i)}{V k_i^2 \Delta k_i} \quad (\text{A11})$$

We see that the errors in the different multipole moments are uncorrelated. For the monopole

$$\langle [\Delta \hat{P}_0(k_i)]^2 \rangle = \frac{2\pi^2 [P(\mathbf{k}) + \sigma_N^2]^2}{V k_i^2 \Delta k_i} \quad (\text{A12})$$

and

$$\langle [\Delta \hat{P}_n(k_i)]^2 \rangle = (2n+1) \langle [\Delta \hat{P}_0(k_i)]^2 \rangle \quad (\text{A13})$$

for the higher multipoles.

We next consider the ratio of the multipoles

$$\hat{\mathcal{R}}_n(k_i) = \frac{\hat{P}_n(k_i)}{\hat{P}_0(k_i)} \quad (\text{A14})$$

We calculate the variance of $\hat{\mathcal{R}}_n(k_i)$ using

$$\Delta \hat{\mathcal{R}}_n(k_i) = \frac{[\Delta \hat{P}_n(k_i)]}{P_0(k_i)} - \frac{P_n(k_i)}{P_0(k_i)} \frac{[\Delta \hat{P}_0(k_i)]}{P_0(k_i)} \quad (\text{A15})$$

whereby

$$\langle [\Delta \hat{\mathcal{R}}_n(k_i)]^2 \rangle = \frac{\langle [\Delta \hat{P}_n(k_i)]^2 \rangle}{P_0^2(k_i)} + \frac{P_n^2(k_i)}{P_0^2(k_i)} \frac{\langle [\Delta \hat{P}_0(k_i)]^2 \rangle}{P_0^2(k_i)} \quad (\text{A16})$$

which gives

$$\langle [\Delta \hat{\mathcal{R}}_n(k_i)]^2 \rangle = [(2n+1) + \mathcal{R}_n^2(k_i)] \frac{\langle [\Delta \hat{P}_0(k_i)]^2 \rangle}{P_0^2(k_i)} \quad (\text{A17})$$

In summary we have a relation between $\delta \mathcal{R}_n$ which is the error in the ratio $\mathcal{R}_n = P_n/P_0$ and the fractional error $\delta P_o/P_o$ of the monopole.

$$\delta \mathcal{R}_n = \sqrt{2n+1 + \mathcal{R}_n^2} \left(\frac{\delta P_0}{P_0} \right) \quad (\text{A18})$$

This provides a rough estimation of possible errors that will be present in the estimations of the ratio of angular moments of 21-cm power spectrum. We plan to take up a more detailed uncertainty analysis in our future work.